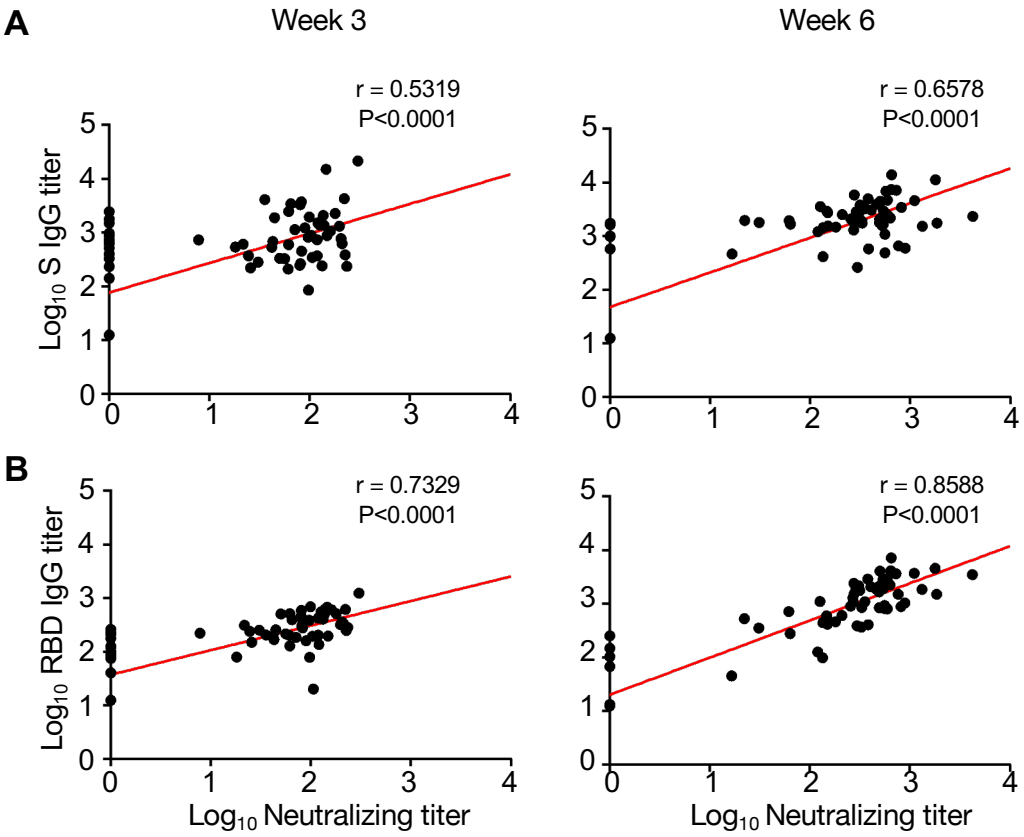

Supplemental Figure 1. Correlation of antibody titers and neutralizing titers. (A,B) Correlations of S- (A) and RBD- (B) binding titers and neutralizing titers at weeks 3 and 6 post vaccination. Red line denote linear regression fit. P and **r** values determined by two-sided Spearman rank test. n=75.

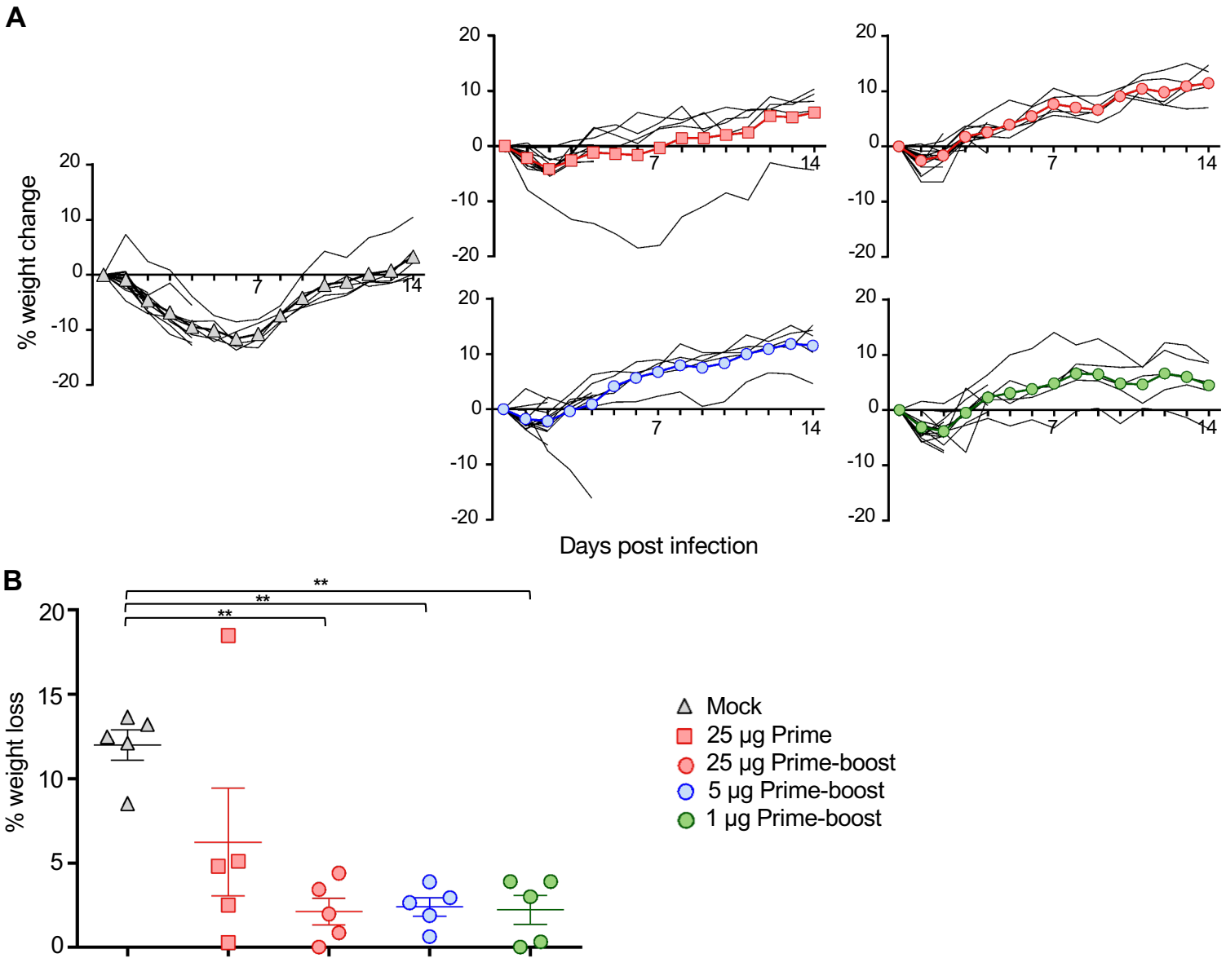

Supplemental Figure 2. Characteristics of clinical disease following SARS-CoV-2 challenge of vaccinated hamsters. (A) Percent weight change in individual animals mock vaccinated (n=15) or prime (25 µg; n=15) or prime-boost (25 µg, 5 µg and 1 µg; n=15 per group) vaccinated with mRNA-1273 over 14 days post infection. Mean weight highlighted by line with color symbols. A weight measure for one hamster in the 25 ug prime-boost group at 2 dpi, the time of euthanasia, was excluded due to a measurement error. (B) Maximum weight loss in vaccinated groups (n=5 per group), excluding animals serially euthanized on days 2 and 4 post challenge. Significance measured by ANOVA with Tukey's correction for multiple comparisons (**P ≤ 0.01). Error bars represent ± SE.

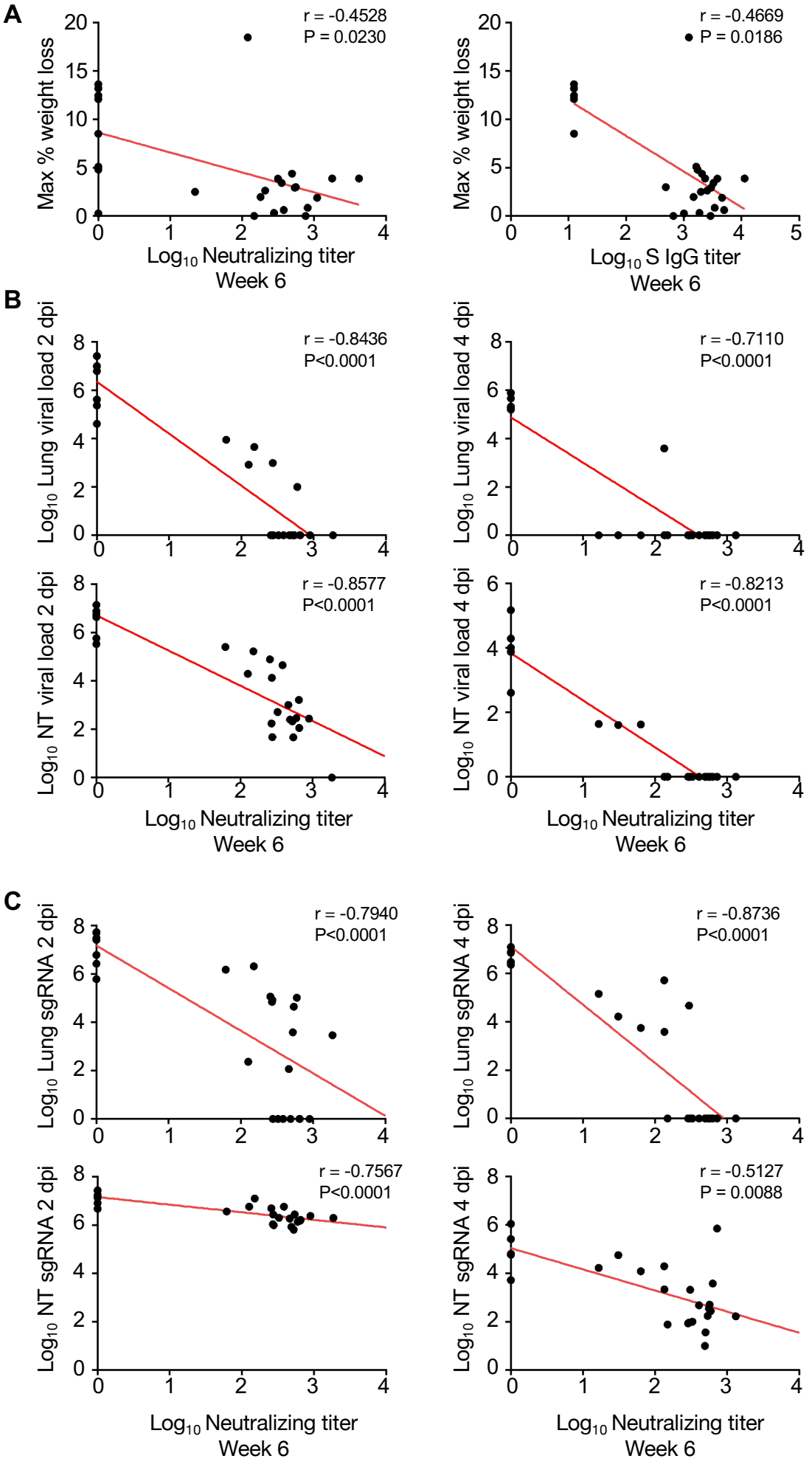

Supplemental Figure 3. Correlation of antibody and neutralizing titers with disease parameters. (A) Correlations of S- binding titers and neutralizing titers at week 6 post vaccination with maximum percentage weight loss excluding hamsters euthanized at 2 and 4 dpi (n=25). Correlations between neutralizing titers at week 6 post vaccination and (B) virus load titers or (C) sgRNA in lungs and nasal turbinates at 2 or 4 dpi (n=25). Red lines denote linear regression fit. P and r values were determined by two-sided Spearman rank test

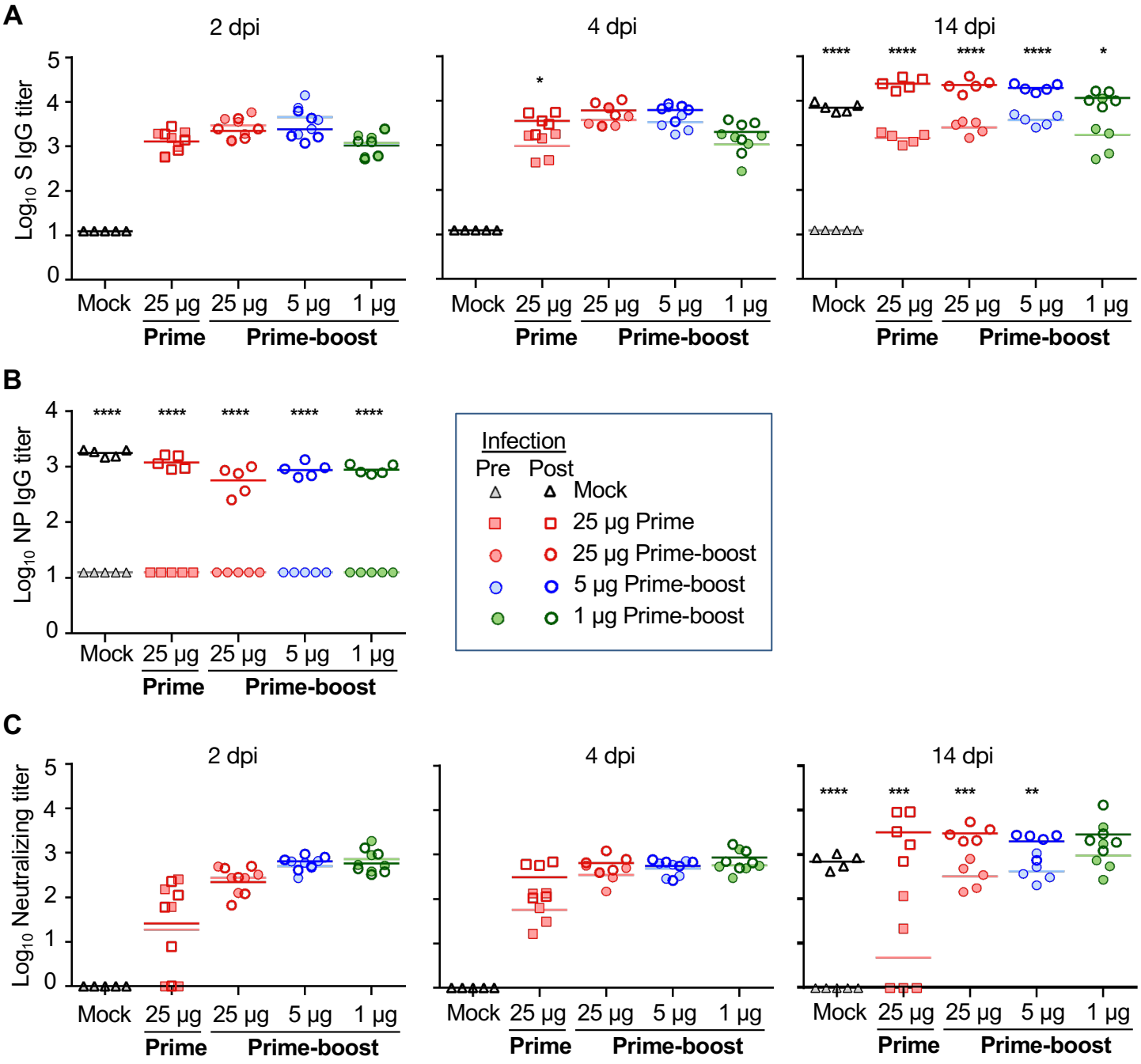

Supplemental Figure 4. Serum antibody responses post SARS-CoV-2. challenge. (A) S-specific serum IgG titers in serum collected pre- (day 41 post-vaccination; shaded symbol) and post-infection (2, 4 and 14 days post-infection (dpi) open symbol. n=5 per group at pre- and post-infection time points), determined by ELISA. (A) S-specific serum IgG titers pre- (day 41 post-vaccination; shaded symbol) and post-infection (2, 4 and 14 days post-infection (dpi) open symbol) determined by ELISA. (B) NP-specific IgG titers in serum collected a day before challenge (day 41) and 14 dpi determined by ELISA. (C) Neutralizing titers in serum collected pre- (day 41 post-vaccination; shaded symbol) and post-infection (2, 4 and 14 dpi; open symbol), determined by plaque reduction assay. Bars denote group means. Significance between pre- and post- infection antibody titers measured by multiple t tests with Holm-Sidak's correction for multiple comparisons (*P ≤ 0.05, **P ≤ 0.01, ***P ≤ 0.001, ****P ≤ 0.0001).

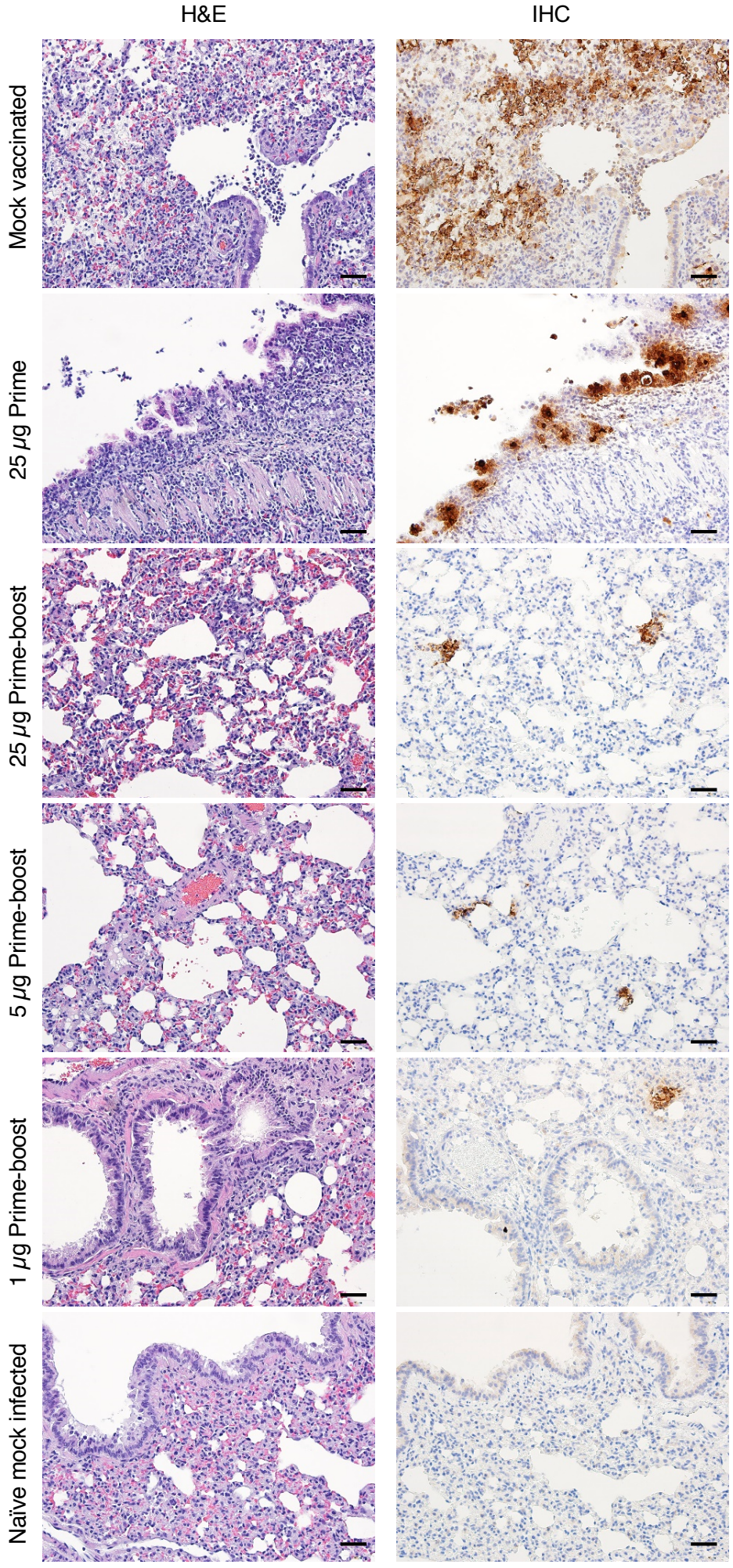

Supplemental Figure 5. Disease following challenge of vaccinated hamsters with SARS-CoV-2
(continued from Fig. 2). Lung sections from mock vaccinated, prime-only and prime-boost vaccinated and naïve mock-infected groups at 4 dpi were stained with H&E, and representative photomicrographs (original magnification ×20 (scale bars, 50 μm) as indicated) from each group with virus antigen (arrowhead) in lungs, stained by IHC.

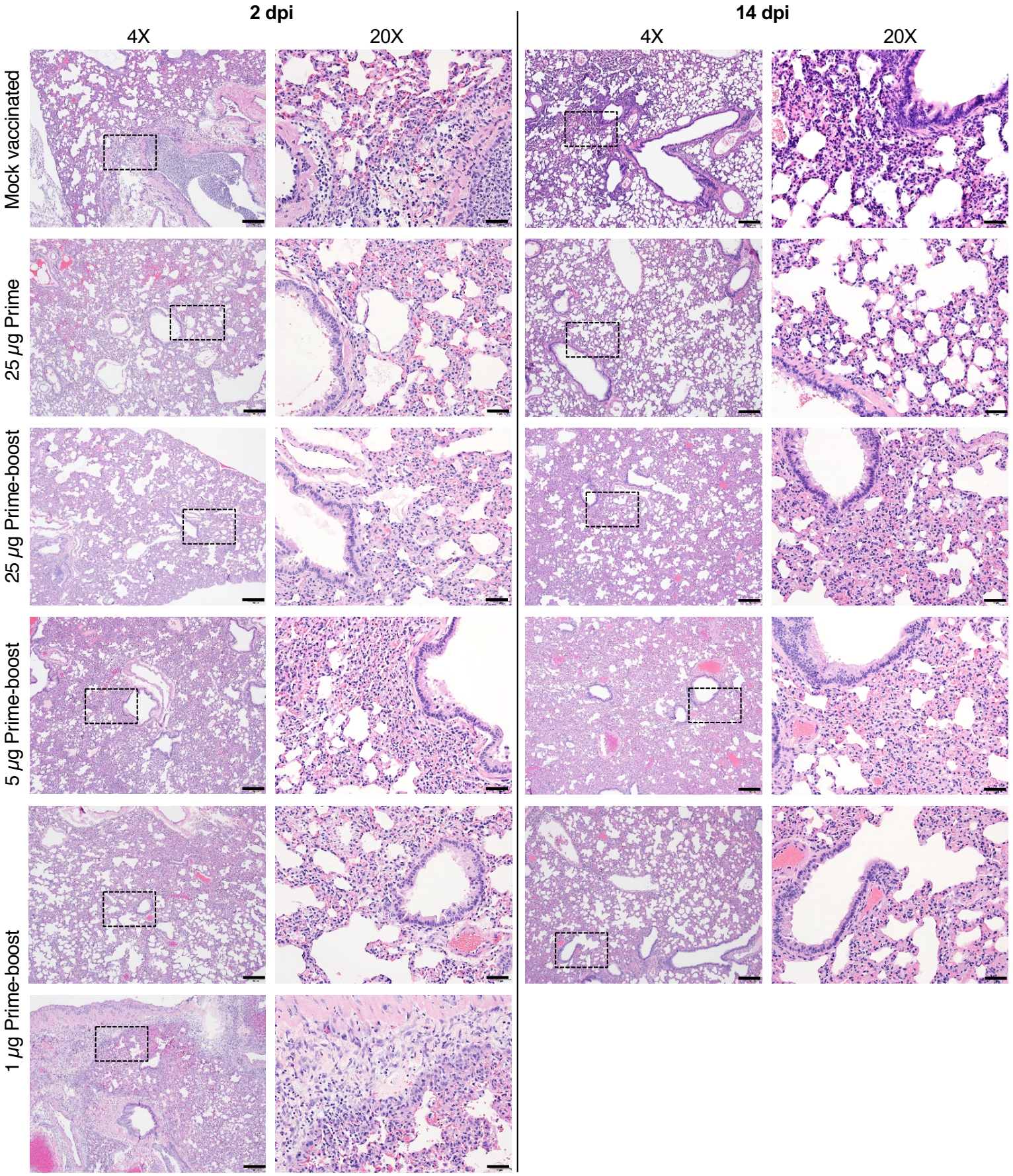

Supplemental Figure 6. Disease following challenge of vaccinated hamsters with SARS-CoV-2 (continued from Fig 2). Lung sections from mock vaccinated, prime-only and prime-boost vaccinated animals at 2 and 14 dpi were stained with H&E, and representative photomicrographs (original magnification ×4 (scale bars, 200 μm) and ×20 (scale bars, 50 μm) as indicated) from each group with virus antigen (arrowhead) in lungs, stained by IHC, are shown.

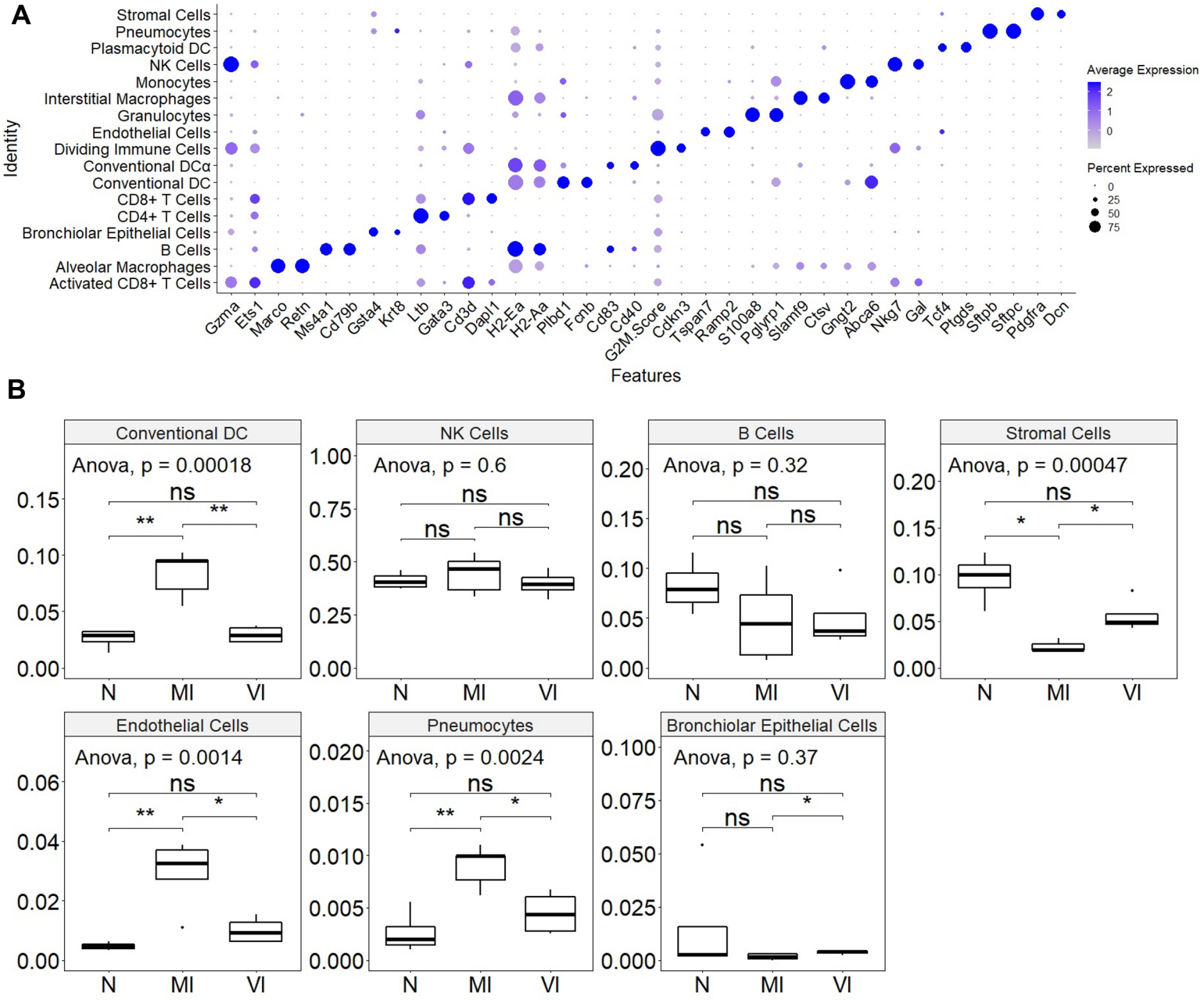

Supplemental Figure 7. **Cell type-specific markers differentiate between cell types; cell-type proportions differ among N, MI and VI pulmonary tissue.** (A) Bubble plot of two top differentiating markers for each cell type. Dividing immune cells are marked by the gene Cdkn3 and the G2M score derived in Seurat. (B) Box plots comparing remaining cell-type proportions observed in each group (N, n=4; MI, n=5; VI, n=4) not shown in Figure 3C The limits of the box reflect the interquartile range (IQR: Q3-Q1) with median shown as horizontal bars. Whiskers extend to 1.5 times the IQR of the box. Outliers outside the 1.5*IQR are shown as individual points. ANOVA and post-hoc Tukey test pairwise comparisons are shown. * p<.05, ** p<.01, ***p<.001, **** p<.0001.

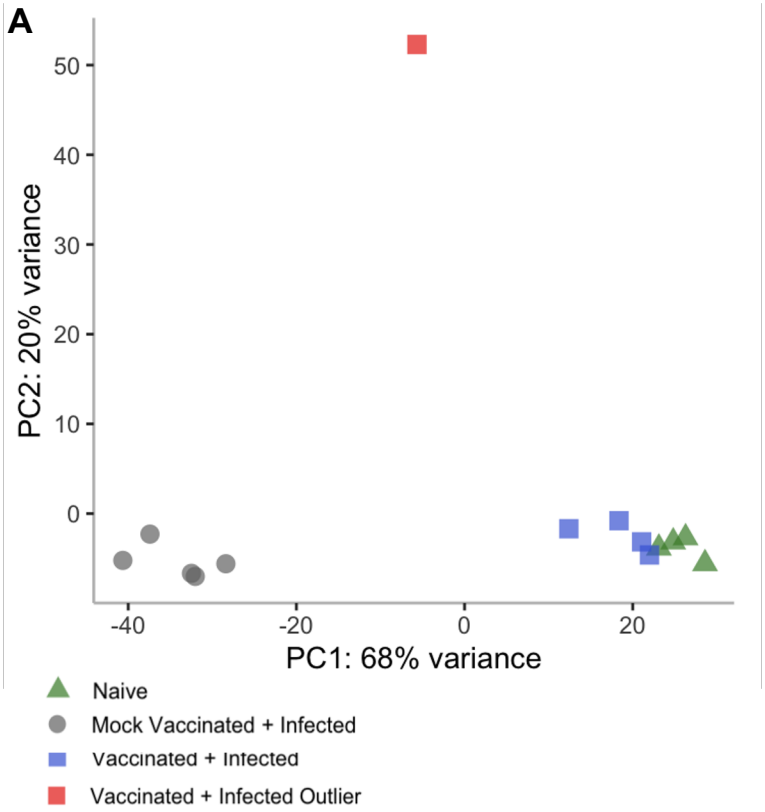

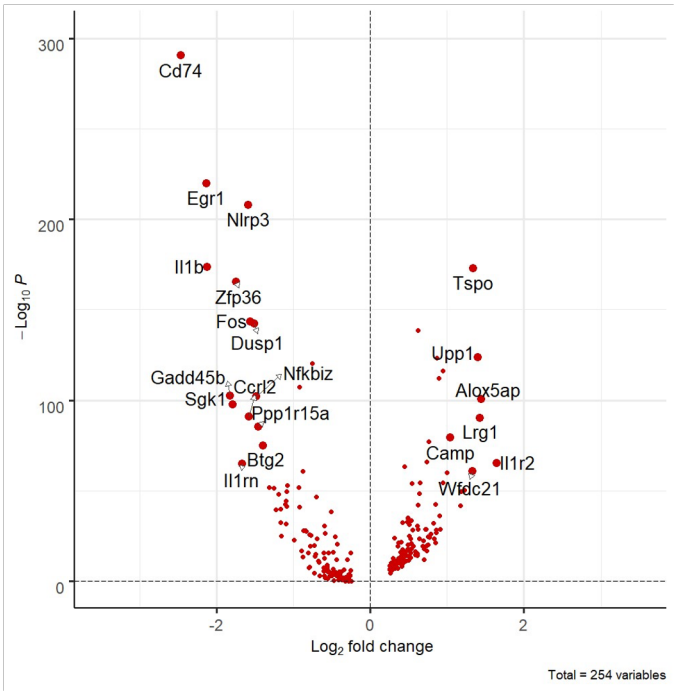

D

Upregulated Pathways

Pathway name	Entities found	Entities Total	Entities ratio	Entities pValue
Neutrophil degranulation	27	480	0.033	8.1E-10
Signaling by RAS mutants	9	54	0.004	8.56E-8
Signaling by moderate kinase activity BRAF mutants	9	54	0.004	8.56E-8
Signaling downstream of RAS mutants	9	54	0.004	8.56E-8
Paradoxical activation of RAF signaling by kinase inactive BRAF	9	55	0.004	9.98E-8
Innate Immune System	43	1,331	0.09	1.21E-7
Signaling by RAF1 mutants	8	49	0.003	5.28E-7
Signaling by high-kinase activity BRAF mutants	8	52	0.004	8.19E-7
Gene and protein expression by JAK-STAT signaling after Interleukin-12 stimulation	9	73	0.005	1.03E-6
Signaling by Interleukins	26	647	0.044	1.2E-6

Downregulated Pathways

Pathway name	Entities found	Entities Total	Entities ratio	Entities pValue
Interleukin-10 signaling	12	86	0.006	8.72E-11
Immune System	59	2,895	0.197	5.2E-9
Signaling by Interleukins	24	647	0.044	2.42E-8
Interleukin-4 and Interleukin-13 signaling	13	216	0.015	2.79E-7
Innate Immune System	32	1,331	0.09	1.84E-6
Cytokine Signaling in Immune system	31	1,332	0.09	5.37E-6
Respiratory electron transport, ATP synthesis by chemiosmotic coupling, and heat production by uncoupling proteins.	9	150	0.01	2.07E-5
NGF-stimulated transcription	6	56	0.004	2.24E-5
Defective CSF2RA causes SMDP4	3	8	0.001	7.54E-5
Defective CSF2RB causes SMDP5	3	8	0.001	7.54E-5

Supplemental Figure 8. Gene regulation in the vaccinated infected VI outlier sample. (A,B) PCA of pseudo-bulk RNA-seq data including all cell types (A) and just granulocytes (B) Colors indicate groups (N, n=4; MI, n=5; VI, n=4). Outlier shown in red. (C) Volcano plot of genes that are differentially expressed (DE) between the outlier sample and the other VI samples (n=4). 270 differentially expressed genes satisfying a logFC threshold of 0.25 and an FDR adjusted p-value of 0.05 were identified: 158 up-regulated, 112 down-regulated. Only DE genes are shown. (D) Upregulated and downregulated Reactome pathways for the outlier vs. the other VI samples (n=4).

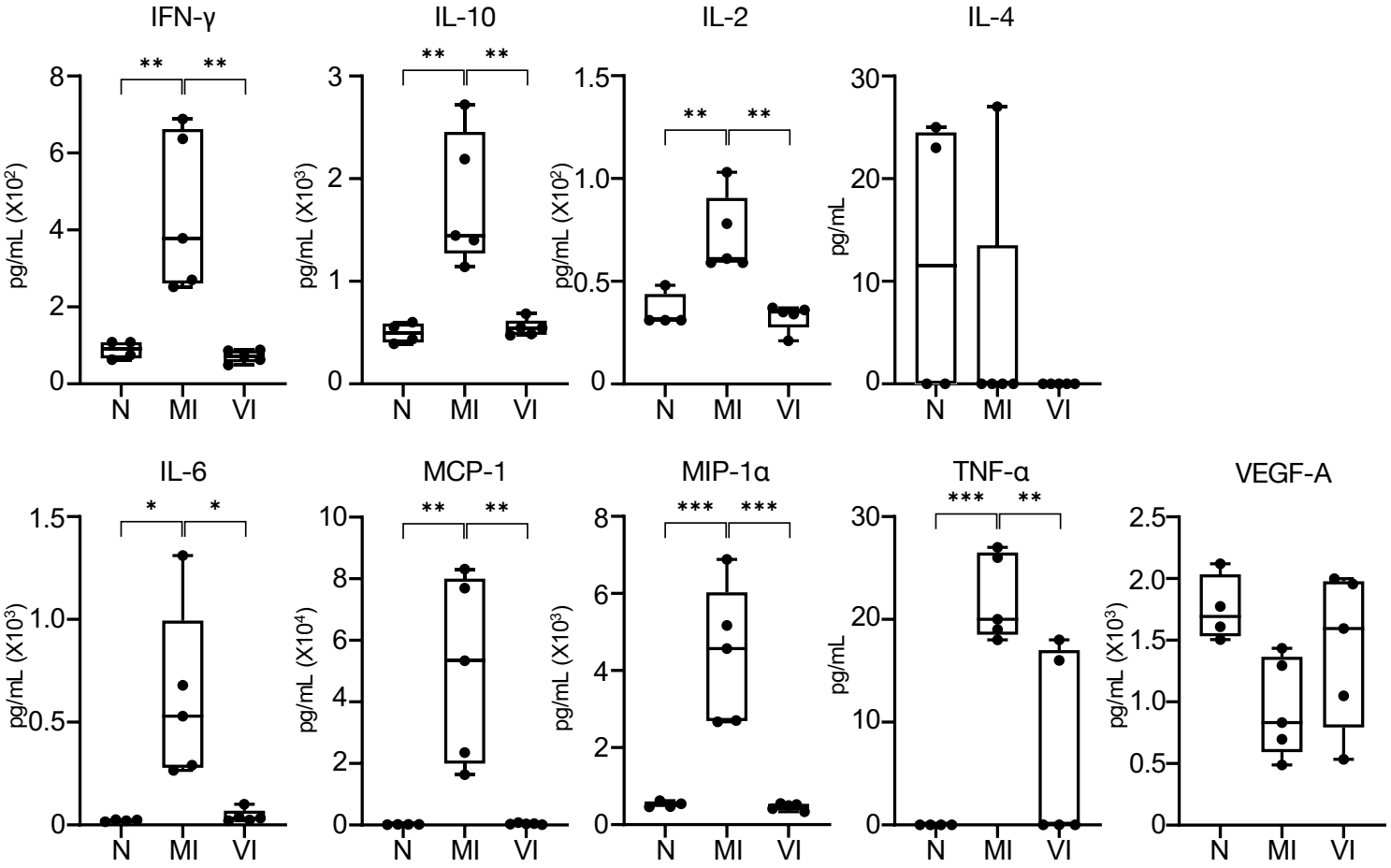

Supplemental Figure 9. Cytokine responses post SARS-CoV-2 challenge. Cytokine levels in lung homogenates from naïve (N; n=4), mock vaccinated-infected (MI; n=5) and 5 µg prime-boost vaccinated-infected (VI; n=5) hamsters collected at day 4 post-infection determined by Hamster MAP assay. Circle symbol represents each hamster. The limits of the box reflect the interquartile range (IQR: Q3-Q1). Bars denote group median. Whiskers extend from min to max value. Significance measured by with Tukey's correction for multiple comparisons (*P ≤ 0.05, **P ≤ 0.01, ***P ≤ 0.001).

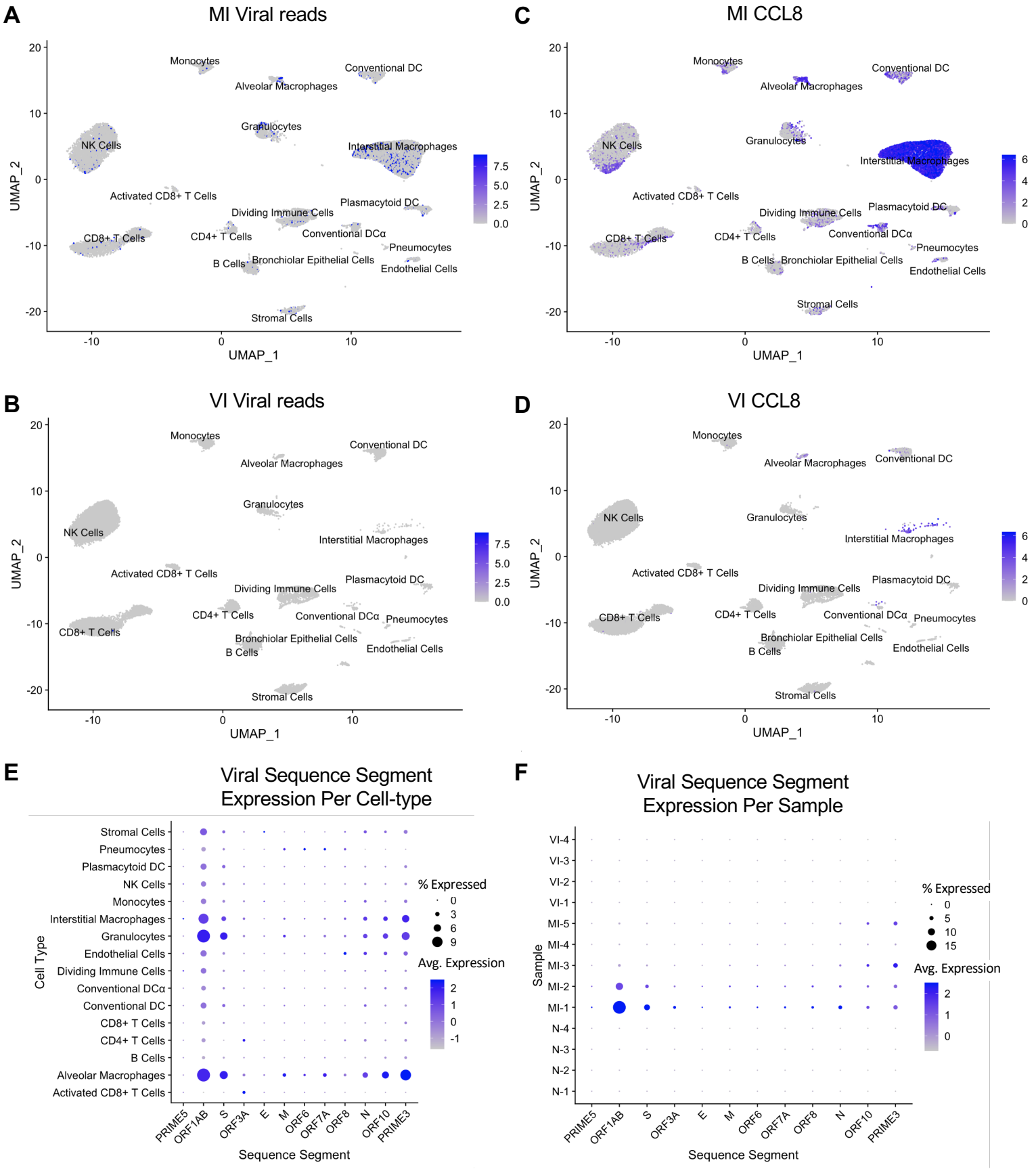

Supplemental Figure 10. Viral sequence segment expression and CCL8 expression from lung tissue single cell RNA-seq. (A-B) Per-cell expression levels of all viral reads in (A) MI (n=5) and (B) VI (n=4) groups visualized in UMAP plot. (C-D) Per-cell expression levels of CCL8 in (C) MI (n=5) and (D) VI (n=4) groups visualized in UMAP plot. (E) Dot plot showing expression of each viral sequence segment in each cell type (including cells only from MI group; n=5). Cell types are only shown if there are more than 20 cells per cell type. (F) Dot plot showing expression of each viral sequence segment in each sample. PRIME5 and PRIME3 represent the 5' and 3' ends, respectively, of the viral genome.

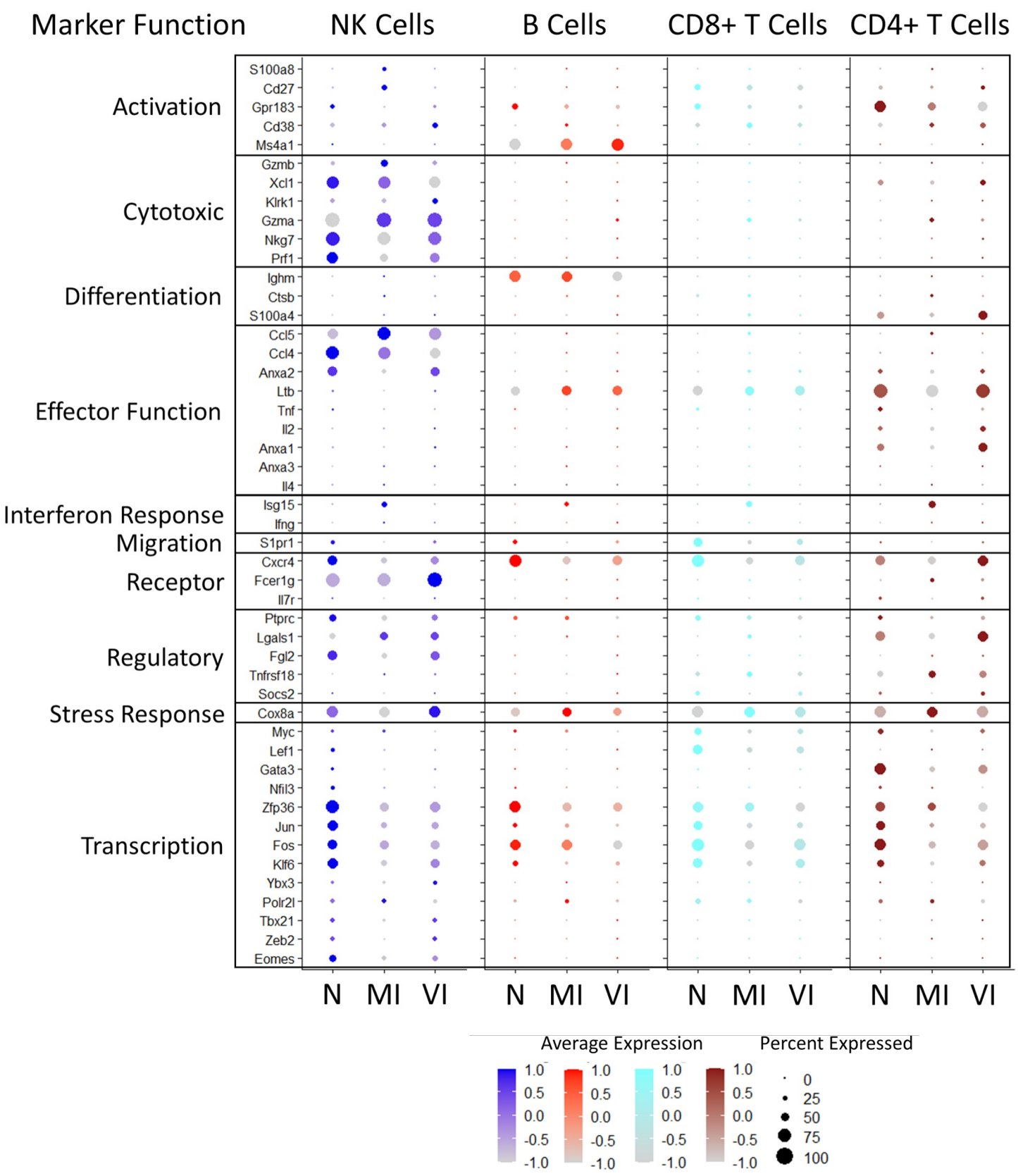

Supplemental Figure 11. Activation marker expression within nondividing lymphocyte cell types. Bubble plot showing scaled expression of lymphocyte marker genes across N (n=4), MI (n=5) and VI (n=4) populations in each sample condition, split by cell type. Genes were selected if they exhibited significant changes in expression across conditions in at least one cell type and are grouped by function. Dot size reflects percent of cells expressing the gene while color density reflects expression levels. Colors for each cell type are the same as in Figure 3.

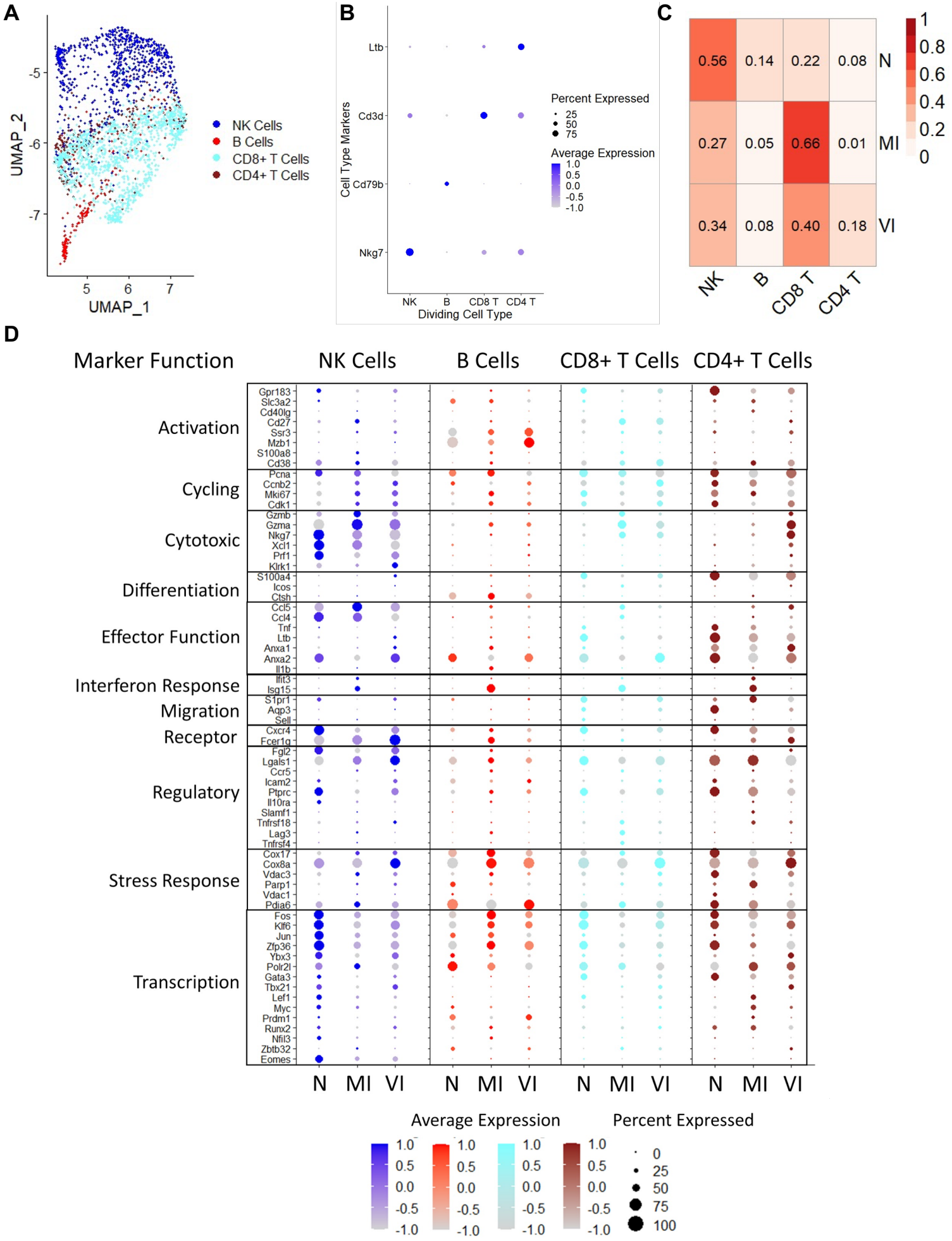
A
UMAP_2
UMAP_1
NK Cells
B Cells
CD8+ T Cells
CD4+ T Cells
B
Cell Type Markers
Ltb
Cd3d
Cd79b
Nkg7
NK
B
CD8 T
CD4 T
Dividing Cell Type
Percent Expressed
Average Expression
C
0.56 0.14 0.22 0.08 N
0.27 0.05 0.66 0.01 MI
0.34 0.08 0.40 0.18 VI
NK
B
CD8 T
CD4 T
D
Marker Function
NK Cells
B Cells
CD8+ T Cells
CD4+ T Cells
Activation
Cycling
Cytotoxic
Differentiation
Effector Function
Interferon Response
Migration
Receptor
Regulatory
Stress Response
Transcription
N MI VI N MI VI N MI VI N MI VI
Average Expression
Percent Expressed

Supplemental Figure 12. Analysis of cell type proportions and activation marker expression within the dividing immune cell cluster. (A) UMAP of dividing immune cell cluster on the same axes as Figure 3A, colored by immune cell types present within the cluster (B) Bubble plot of expression of cell type specific markers for the dividing immune cell subtypes. (C) Table of dividing immune cell type proportions within N (n=4), MI (n=5) and VI (n=4) groups. (D) Bubble plot of gene expression levels for lymphocyte markers in N (n=4), MI (n=5) or VI (n=4) groups, split by dividing cell type. Genes were selected if they exhibited significant changes in expression across conditions in at least one dividing cell type and are grouped by function. Dot size reflects percent of cells expressing the gene while darker shades reflect increased average expression levels. Colors for each cell type are the same as in Figure 3.

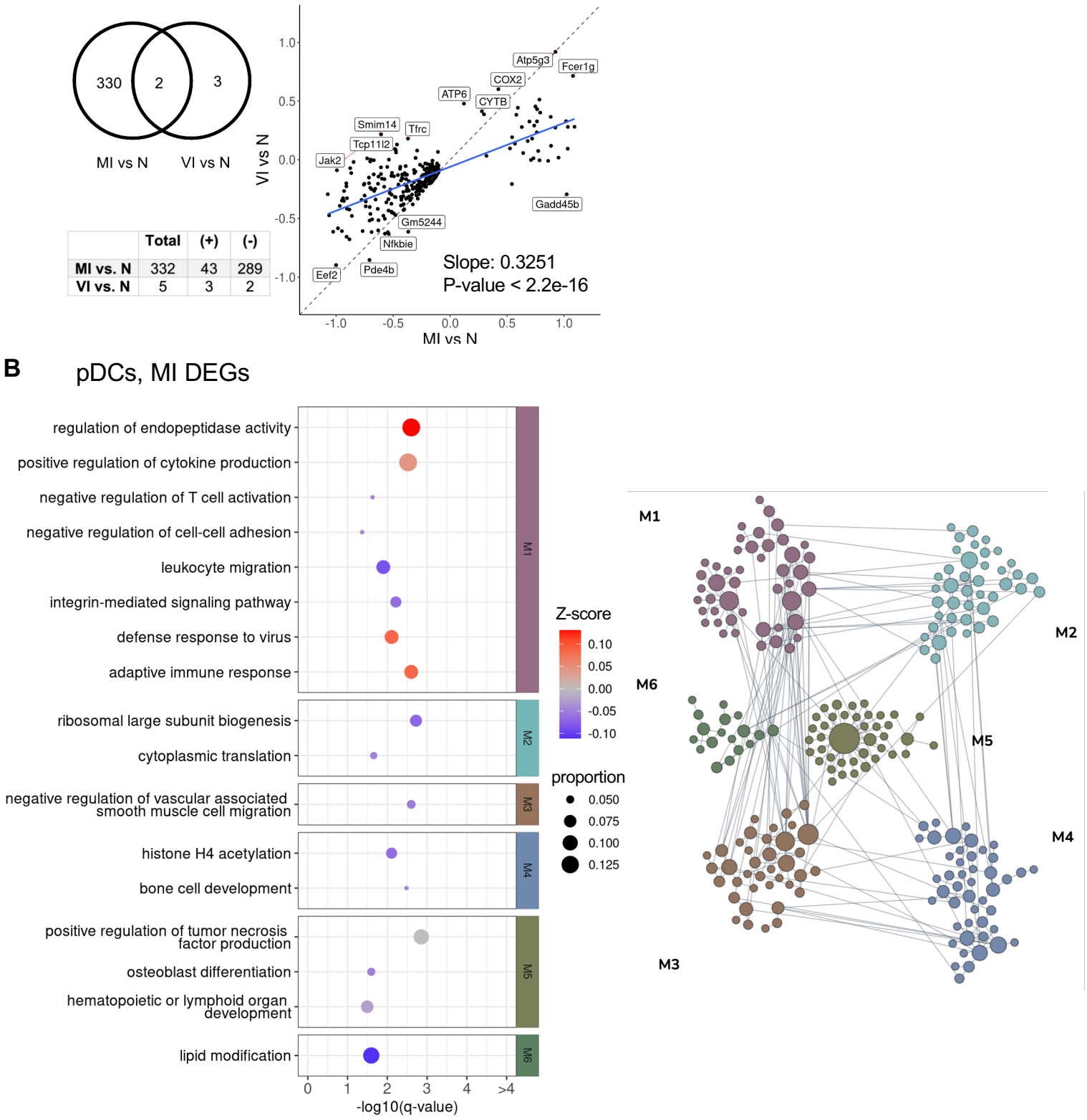

Supplemental Figure 13. Venn diagram, scatterplot, and network-based functional interpretation of DEGs of MI vs. N comparison in plasmacytoid DC (pDCs). (A) The table below the Venn diagram indicates the total number of DEGs, number of up-regulated DEGs (positive logFC), and number of down-regulated DEGs (negative logFC) in each of the two comparisons. Scatter plot of the logFC of the union of DEGs of the two comparisons in corresponding cell types, i.e. the union of DEGs as in the Venn diagram. Linear regression model was fitted to the scatter plot. Adjusted R^2 is 0.5098. (B) Functional interpretations of DEGs MI vs. N for pDCs. The bubble plot (left) shows key pathways enriched in each functional module (M) within the network plot for DEGs from MI vs. N comparison (right). (Left) The color of each bubble represents the Z-score for each pathway which defines the directional tendency of regulation. Bubble size corresponds to the proportion of DEGs in each pathway relative to the total number of DEGs within M. (Right) In the network plots, DEGs are clustered into M/gene communities based on functional relatedness in the lung tissue. Each DEG is represented by a node within M and each edge represents a functional association between the pair of DEGs. A node with a larger size reflects a higher degree of connectivity in the network. N: n=4; MI: n=5 and VI: n=4.

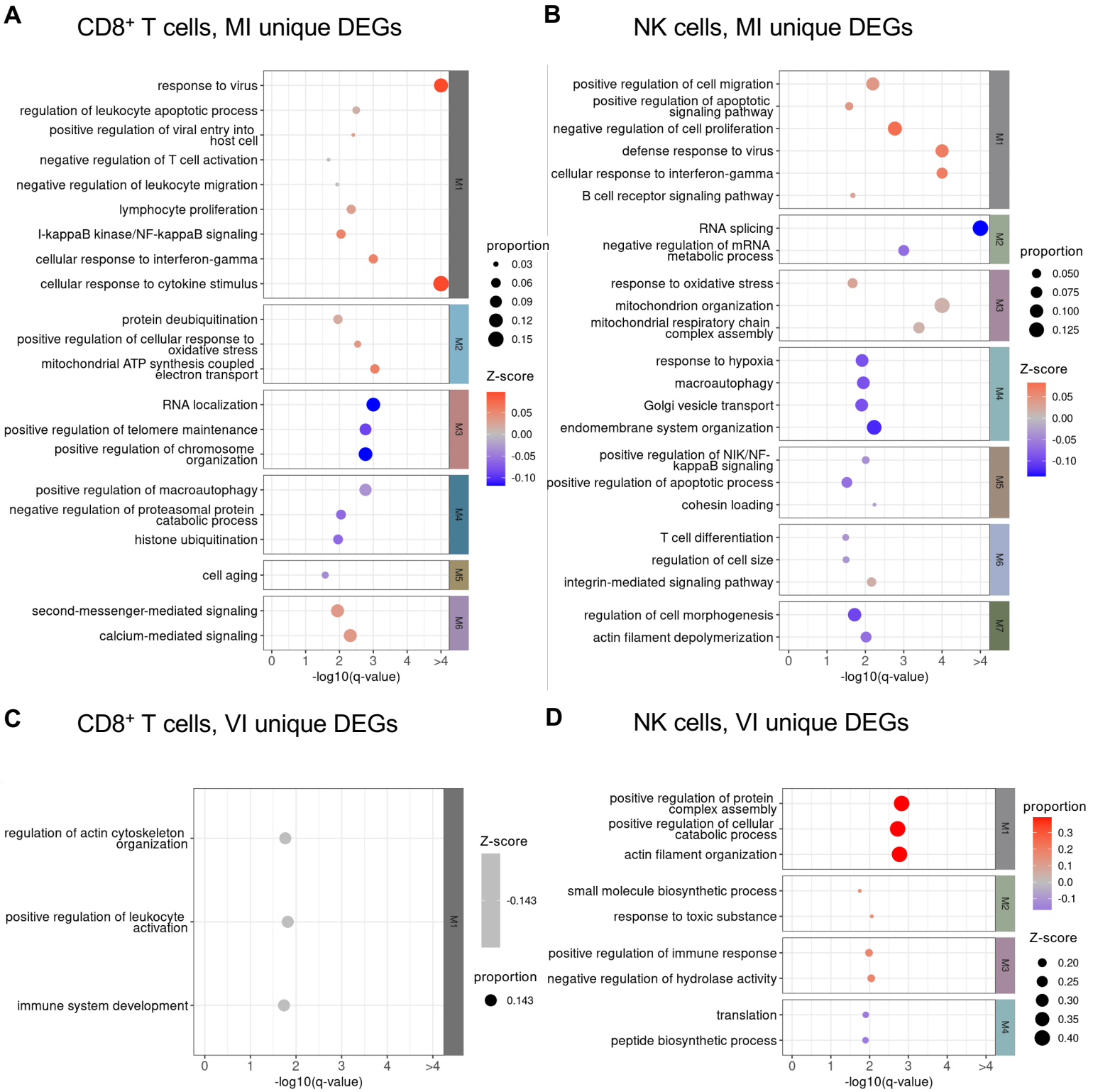

Supplemental Figure 14. Bubble plot showing the network-based functional interpretation of unique DEGs in each of the MI vs. N and VI vs. N comparisons in CD8+ T cells and NK cells. (A-D) Bubble plot of key pathways enriched in each functional module (M) within the functional network for DEGs unique to (A,B) MI vs. N or (C,D) VI vs. N comparisons in (A,C) CD8+ T cells and (B,D) NK cells, i.e. fall outside the Venn diagram overlap in Fig. 5. The color of each bubble shows the direction of regulation in MI or VI ('red' for up-regulation and 'blue' for down-regulation). Size represents to the proportion of DEGs in each pathway relative to the total number of DEGs within M. M/gene communities were identified by clustering DEGs based on their functional relatedness in the lung tissue. N: n=4; MI: n=5 and VI: n=4.

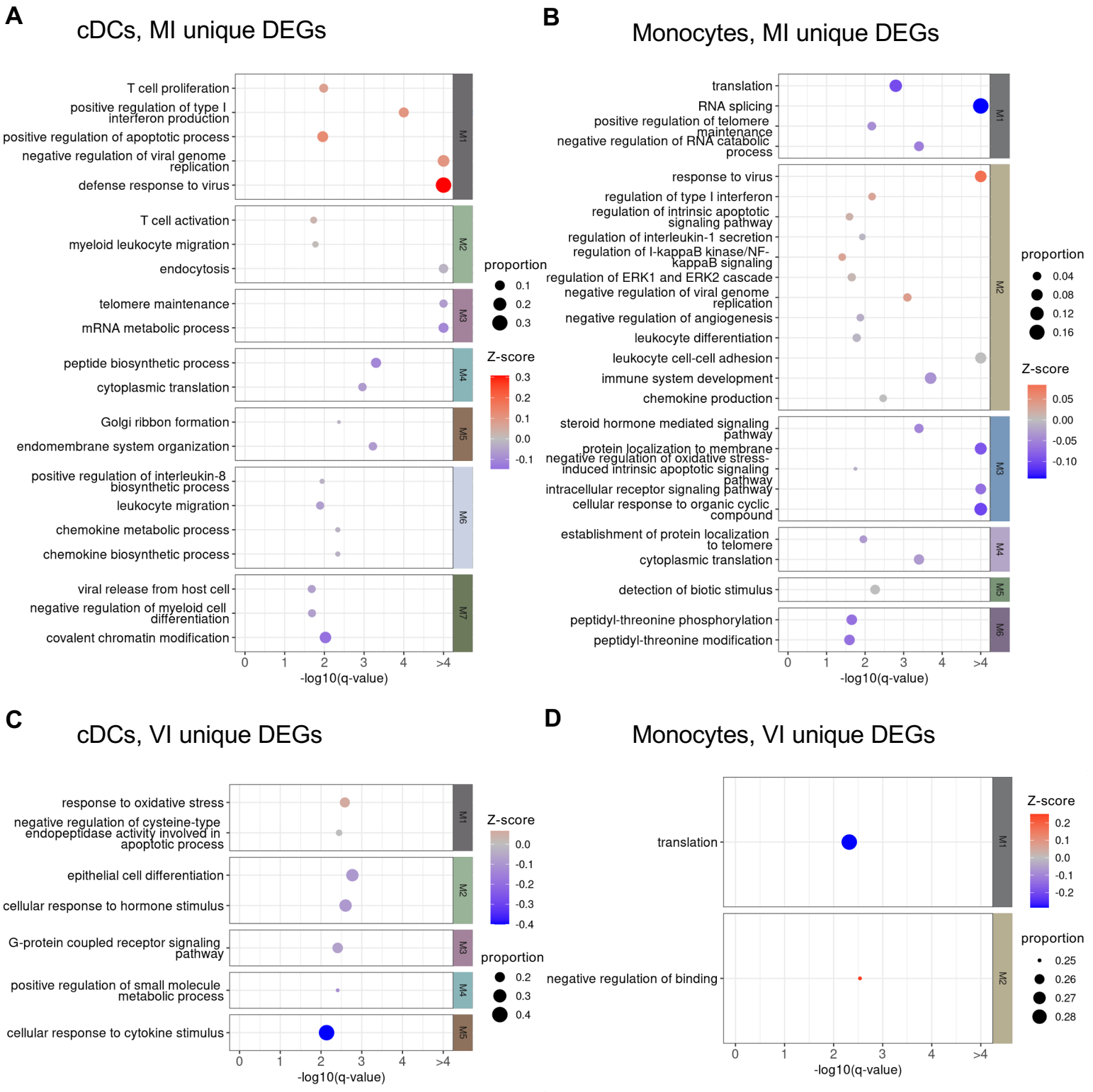

Supplemental Figure 15. Bubble plot showing the network-based functional interpretation of unique DEGs in each of the MI vs. N and VI vs. N comparisons in cDCs and monocytes. (A-D) Bubble plot of key pathways enriched in each functional module (M) within the functional network for DEGs unique to (A,B) MI vs. N or (C,D) VI vs. N comparisons in (A,C) cDCs cells and (B,D) monocytes, i.e. fall outside the Venn diagram overlap in Fig. 5. The color of each bubble shows the direction of regulation in MI or VI ('red' for up-regulation and 'blue' for down-regulation). Size represents to the proportion of DEGs in each pathway relative to the total number of DEGs within M. M/gene communities were identified by clustering DEGs based on their functional relatedness in the lung tissue. N: n=4; MI: n=5 and VI: n=4.

SUPPLEMENTAL METHODS

Human convalescent-phase serum

Human convalescent sera (n = 6) were obtained from adults between 18 and 55 years old with mild (*n* = 2), medium (*n* = 2), and severe (n = 2) COVID-19 and a history of laboratory-confirmed SARS-CoV-2 infection 1 to 2 months before providing specimens. In addition, SARS-CoV-2 naïve sera samples (*n* = 3) were also included in analyses. These specimens were obtained from Aalto Bio Reagents Ltd.

ELISA

S, RBD or nucleocapsid proteins (1µg/mL, Sino Biological) were coated onto 96-well plates for 16 h. Plates were then blocked with SuperBlock (Pierce). Five-fold serial dilutions of hamster serum were then added to the plates (assay diluent – PBS + 0.05% Tween-20 + 5% goat serum) and incubated for 2 hours at 37°C. Bound antibodies were detected with HRP-conjugated goat anti-hamster IgG (1:10,000 Abcam Cat No. ab7146). Following the addition of TMB substrate (SeraCare) and TMB stop solution (SeraCare), the absorbance was measured at OD 450 nm. Titers were determined using a four-parameter logistic curve fit in GraphPad Prism (GraphPad Software, Inc.) and defined as the reciprocal dilution at approximately OD450nm = 1.5 (normalized to a hamster standard on each plate).

SARS-CoV-2 neutralization assay

Two-fold serial dilutions of heat-inactivated serum at an initial dilution of 1:10 were prepared in serum-free MEM media and incubated with SARS-CoV-2-mNG for 1 hour at 37°C at a final concentration of 100 PFU. Virus-serum mixtures then were absorbed onto Vero-E6 monolayers in black optical 96 well plates for 1 hour at 37°C and replaced with MEM/Methylcellulose/2% FBS overlay. After 2 days of incubation at 37°C in humidified 5% CO2, neon green plaques were visualized and counted. Neutralization titers at an end point of 60% plaque reduction were determined.

Analysis of viral load by plaque assay

The right lung and nasal turbinates were homogenized in Leibovitz L-15 medium (Thermo Fisher Scientific)/10% FBS/1X Antibiotic-Antimycotic (Thermo Fisher Scientific) using the TissueLyser II bead mill (Qiagen) and 5 mm stainless steel beads (Qiagen) and briefly centrifuged. Ten-fold serial dilutions of homogenates were prepared in serum free MEM media and absorbed on Vero-E6 (ATCC) monolayers in 48 well plate for 1 hour at 37°C. The virus inoculum was removed replaced with an overlay of MEM/methylcellulose/2% FBS. After 3 days, plaques were immunostained with a human monoclonal antibody cocktail specific for the S protein (kindly provided by Distributed Bio (South San Francisco, CA); Clones DB_A03-09, 12; DB_B01-04, B07-10, 12; DB_C01-05, 07, 09, 10; DB_D01, 02; DB_E01-04, 06, 07; DB_F02-03) and an anti-human IgG HRP conjugated secondary antibody (Sera Care Cat No.5220-0456). Plaques were counted and virus load per gram tissue was determined.

Histopathology

Lung samples were processed per a standard protocol for histological analysis. Briefly, the lower left lung lobe was fixed in 10% neutral buffered formalin, embedded in paraffin, sectioned at 5 µm and stained with Hematoxylin and Eosin (H&E) for routine histopathology. Samples were evaluated by a board-certified veterinary pathologist in a blinded manner. Sections were examined under light microscopy using an Olympus BX51 microscope and photographs were taken using an Olympus DP73 camera. Representative sections were displayed.

Immunohistochemistry

Staining of hamster lung sections was done using the Bond RX automated system with the Polymer Define Detection System (Leica) as per manufacturer's protocol. Tissue sections were dewaxed with Bond Dewaxing Solution (Leica) at 72^{o}C for 30 min then subsequently rehydrated with graded alcohol washes and 1x Immuno Wash (StatLab). Heat-induced epitope retrieval (HIER) was performed using Epitope Retrieval Solution 1 (Leica), heated to 100^{o}C for 20 min. A peroxide block (Leica) was applied for 5 min to quench endogenous peroxidase activity prior to applying the SARS-CoV-2 antibody (1:2000, GeneTex, GTX135357). Antibodies were diluted in

Background Reducing Antibody Diluent (Agilent). The tissue was subsequently incubated with an anti-rabbit HRP polymer (Leica) and colorized with 3,3'-Diaminobenzidine (DAB) chromogen for 10 min. Slides were counterstained with hematoxylin and representative sections were shown.

Analysis if cytokines in the lungs

Right lung homogenates collected at 4 dpi from the N (*n* = *4*), MI (*n* = *5*) and 5 μg prime-boost (VI, *n* = 5) groups were analyzed for cytokines by the Hamster MAP 1.0 multiplex immunoassay system at Ampersand Biosciences.

Pseudo-bulk RNA-seq data analysis

Principal component analysis (PCA) plots highlighting the differences between the outlier VI sample and the other samples both overall and specifically within granulocyte cells were generated with the prcomp function in the R package ggfortify. Within granulocytes, differential expression analysis was conducted between the outlier VI sample and the remaining VI samples. DEGs with FDR < 0.05 and absolute log FC > 0.25 were selected as significant. Pathway analysis on the up-regulated and down-regulated DEGs, respectively, was performed with reactome with the top 10 enriched pathways shown.

Supplemental Table 1. Metagenomic Analysis of all 14 samples: selected classification results

Group	Hamster ID	% Mapped to Bacteria and Virus	NCBI Taxon ID	Taxon Name
Naive	N1	0.04	44283	Pasteurella multocida susbsp. Multocida
	N2	0.04	44283	Pasteurella multocida susbsp. Multocida
	N3	0.04	44283	Pasteurella multocida susbsp. Multocida
	N4	0.04	44283	Pasteurella multocida susbsp. Multocida
Mock Vaccinated + Infected	M1	0.04	44283	Pasteurella multocida susbsp. Multocida
		0.16	2697049	Severe acute respiratory syndrome coronavirus 2
	M2	0.04	44283	Pasteurella multocida susbsp. Multocida
		0.05	2697049	Severe acute respiratory syndrome coronavirus 2
	M3	0.03	44283	Pasteurella multocida susbsp. Multocida
		0.03	2697049	Severe acute respiratory syndrome coronavirus 2
	M4	0.03	44283	Pasteurella multocida susbsp. Multocida
		0.005	2697049	Severe acute respiratory syndrome coronavirus 2
	M5	0.02	44283	Pasteurella multocida susbsp. Multocida
		0.02	2697049	Severe acute respiratory syndrome coronavirus 2
Vaccinated + Infected	V1	0.04	44283	Pasteurella multocida susbsp. Multocida
	V2	0.03	44283	Pasteurella multocida susbsp. Multocida
	V3	0.03	44283	Pasteurella multocida susbsp. Multocida
	V4	0.02	44283	Pasteurella multocida susbsp. Multocida
	V5	0.02	44283	Pasteurella multocida susbsp. Multocida

Summary of selected metagenomic analysis of all 14 samples in MI, VI and N groups to identify the presence of additional microbial infections beyond SARS-CoV-2.

Supplemental Table 2. Inflammation and viral antigen in lungs of mRNA-1273 vaccinated hamsters following SARS-CoV-2 infection

Vaccine	H&E (inflammation)			IHC (SARS-CoV-2 antigen)
	2 dpi	4 dpi	14 dpi	4 dpi
Mock vaccinated-infected	+/- i	+ pv/pbr F	+ pv/pbr	+++
	+/- i	++ pv/pbr F	++ pv/pbr, i	+++
	+ i, aw	++ pv/pbr F	+ pv/pbr	++
	++ i, aw	+++ pv/pbr F	++ pv/pbr, i	++
	+ i, aw	+++ pv/pbr F	+ pv/pbr	+++
25 µg Prime	++ i	+ pv/pbr F	+/- i	+
	+/- i	+ pv/pbr F	+/- i	+/- to +
	+/- i	+ pv/pbr F	+/- i	+
	+ i	+ pv/pbr F	+/- i	+
	+i	++ pv/pbr F, edema and fibrin	+/- i	++
25 µg Prime-boost	+/- i	+ i	++ i	-
	+/- i	+ i	+ i	-
	+/- i	+ i	++ i	+/-
	++ i	+/- i	+ i	+/-
	+ i	+ i	++ i	-
5 µg Prime-boost	+ i	+ i	+ i	+/-
	++ i	+/- i	+ i	-
	+/- i	+/- i	+/- i	+/-
	+ i	+/- i	++ i	-
	-	+ i	++ i	+/-
1 µg Prime-boost	+ i	+ i	+ i	+/- to -
	++ i	+/- i	++ i	+/- to -
	+ i	++ pv/pbr F/i	+ i	++
	+/- i	+/- i	+ i	-
	+++ i, edema, rare hemorrhage	+/i	+i	+/- to -
Naïve (Mock infected)	na	+ i	na	-
	na	+++ i	na	-
	na	++ i	na	-
	na	++ i	na	-

Inflammation scoring

Inflammation definitions: focal/multifocal **(F)**, interstitial **(i)** or a combination of both **(F/i), aw** = airway, pv/pbr = perivascular/peribronchiolar

Inflammation minimal to absent = -

<10% (tissue affected) = +/-

>10-<25% = +

>26-<50% = ++

>50%= +++

COVID-19 viral Antigen (Ag) scoring

Minimal - absent = -

Minimally abundant (but clearly present) = +/-

Mildly abundant = +

Moderately abundant =++

Abundant = +++

Supplemental Table 3. Differential gene expression analysis in CD8+ T cells, NK cells, cDCs, pDCs and monocytes, comparing MI vs. VI groups

CD8+ T cell, MI vs. VI DEGs				
Modules	# of genes	Direction	Enriched pathways	q-values
1	53	up	NADH dehydrogenase complex assembly	<1e-04
			Mitochondrion organization	<1e-04
2	20	down	Cytoplasmic translation	<1e-04
			Peptide biosynthetic process	<1e-04
			Protein localization to membrane	<1e-04
3	64	up	Defense response to virus	<1e-04
			Response to interferon-gamma	0.0002
			Leukocyte chemotaxis	0.0002
			Positive regulation of interleukin-10 secretion	0.001
			Response to interleukin-1	0.0017
			Leukocyte cell-cell adhesion	0.0027
4	64	down	Regulation of mRNA splicing, via spliceosome	0.0009
			Response to dsRNA	0.0016
			Regulation of gene silencing by RNA	0.0024
5	39	up	Activation of MAPKKK activity	0.0018
			Negative regulation of JAK-STAT cascade	0.003
			Regulation of interleukin-2 production	0.009
		down	Positive regulation of apoptotic process	0.0003
			Mitotic cell cycle arrest	0.0018
6	25	up	lymphocyte mediated immunity	0.0149
			Positive regulation of MAP kinase activity	0.0245

NK cell, MI vs. VI DEGs				
Modules	# of genes	Direction	Enriched pathways	q-values
1	44	up	Negative regulation of viral process	<1e-04
			Defense response to virus	<1e-04
			Response to tumor necrosis factor	0.0004
			Response to interferon gamma	0.0006
			Response to interleukin-1	0.0009
			Macrophage chemotaxis	0.0016
	47	down	Muscle cell migration	0.0009
			Regulation of fibroblast proliferation	0.0013
			Cell cycle arrest	0.0021
2	13	down	Exocytosis	0.0002
			Leukocyte cell-cell adhesion	0.0004
			Leukocyte migration	0.0005
			Positive regulation of leukocyte activation	0.002
3	38	up	Regulation of protein catabolic process	0.0002
			Translation	0.0003
			Peptide biosynthetic process	0.0003
	39	down	Regulation of oxidative stress-induced cell death	0.0263
			Positive regulation of apoptotic process	0.0324
4	77	down	Natural killer cell chemotaxis	0.0004
			Leukocyte activation	0.0009
			Leukocyte migration	0.001
			Immune system development	0.0021
			Leukocyte mediated cytotoxicity	0.0077
			Cell adhesion mediated by integrin	0.0325
5	89	down	RNA splicing	0.0011
			Regulation of protein localization to membrane	0.0014
			Cellular response to hypoxia	0.0198
6	31	down	Regulation of actin filament-based process	0.0009
			Actin cytoskeleton organization	0.089
			Bone development	0.0116
7	52	down	Positive regulation of nuclease activity	0.0025
			Regulation of telomere maintenance	0.0414
			Endomembrane system organization	0.0419

cDC, MI vs. VI DEGs				
Modules	# of genes	Direction	Enriched pathways	q-values
1	54	up	Response to virus	<1e-04
			Positive regulation of cytokine production	<1e-04
			Negative regulation of viral process	<1e-04
			Positive regulation of cytokine secretion	<1e-04
			I-kappaB kinase/NF-kappaB signaling	<1e-04
			Regulation of type I interferon production	<1e-04
			Cellular response to cytokine stimulus	0.0002
2	108	down	Peptide biosynthetic process	<1e-04
			Cytoplasmic translation	<1e-04
			NADH dehydrogenase complex assembly	<1e-04
3	125	down	Membrane raft organization	0.0002
			Response to hormone	0.001
			Viral entry into host cell	0.0012
4	91	down	Integrin-mediated signaling pathway	0.0002
			Leukocyte cell-cell adhesion	0.0022
			Myeloid leukocyte mediated immunity	0.0052
			Cell morphogenesis	0.0123
5	29	up	Cellular response to interleukin-1	0.0067
			Negative regulation of JAK-STAT cascade	0.0073
			Positive regulation of T cell activation	0.014
	32	down	Positive regulation of apoptotic process	0.002
			Response to hypoxia	0.008
6	118	down	Positive regulation of autophagy	0.011
			Protein localization to plasma membrane	0.016
7	50	down	mRNA splicing, via spliceosome	0.025

pDC, MI vs. VI DEGs				
Modules	# of genes	Direction	Enriched pathways	q-values
1	59	up	Defense response to virus	<1e-04
			Negative regulation of viral process	0.0004
			Response to interferon-gamma	0.001
			Antigen processing and presentation of endogenous peptide antigen via MHC class I	0.0014
			Positive regulation of cytokine production	0.0026
2	104	down	Translation	<1e-04
			Peptide metabolic process	<1e-04
			Mitochondrial respiratory chain complex assembly	0.005
3	30	down	Leukocyte chemotaxis	0.0001
			Exocytosis	0.0008
			Lymphocyte migration	0.0011
			Leukocyte degranulation	0.007
4	27	up	positive regulation of apoptotic process	0.0001
			activation of protein kinase activity	0.0007
	36	down	smooth muscle cell proliferation	0.0016
5	51	down	Anion transport	0.01
			Positive regulation of GTPase activity	0.03
6	17	down	Regulation of macroautophagy	0.01
			Histone acetylation	0.02

Monocytes, MI vs. VI DEGs				
Modules	# of genes	Direction	Enriched pathways	q-values
1	67	up	Immune effector process	<1e-04
			Defense response to virus	<1e-04
			Positive regulation of leukocyte activation	<1e-04
			Positive regulation of interleukin-10 secretion	<1e-04
			Negative regulation of viral process	<1e-04
			Regulation of monocyte chemotaxis	<1e-04
2	45	up	Cytoplasmic translation	<1e-04
			Peptide biosynthetic process	<1e-04
			Mitochondrial respiratory chain complex assembly	0.0252
3	95	down	Regulation of RNA splicing	0.0002
			Regulation of viral-induced cytoplasmic pattern recognition receptor signaling pathway	0.0012
			Positive regulation of gene silencing by miRNA	0.0014
			Regulation of cytoskeleton organization	0.0015
			Leukocyte tethering or rolling	0.0015
			Cellular response to dsRNA	0.0018
4	54	down	Cell cycle arrest	0.0002
			Vasculature development	0.0004
			Angiogenesis	0.001
			Cellular response to hypoxia	0.042
5	22	down	Positive regulation of cellular extravasation	0.0002
			Detection of biotic stimulus	0.0015
			Positive regulation of cell migration	0.017